Comparative Analysis of a Detailed and an Average VARC DCCB model in MTDC Systems

Shetgaonkar, Ajay; Liu , Siyuan ; Popov, Marjan

DOI
10.1109/PESGM48719.2022.9916949

Publication date
2022

Document Version
Final published version

Published in
Proceedings of the 2022 IEEE Power & Energy Society General Meeting (PESGM)

Comparative Analysis of a Detailed and an Average VARC DCCB model in MTDC Systems

Ajay Shetgaonkar, Siyuan Liu and Marjan Popov

***Abstract*-- Direct current circuit breaker (DC CB) is the key component to provide reliable operation of Multi-terminal Direct Current (MTDC) system. Fast, effective and accurate DC CB models are needed for system-level studies. Due to large number of components in the DC CB, its detailed modeling is needed in order to simulate current interruption process correctly. However, the simulation time may be longer depending on the network complexity. This paper proposes an average model which is compared to a detailed model of a Voltage-source-converter resonant current (VARC) DC CB in an MTDC system in terms of its performance and computation time for two typical simulation cases. The average and the detailed model are modelled and simulated in PSCAD/EMTDC environment. An accurate response of the average model during fast transient event is presented, showing additional computational advantage.**

***Keywords*: Average model, VARC DC circuit breaker, HVDC, MTDC.**

I. Introduction

THE reliable operation of an MTDC system depends upon detection of a DC fault and its current interruption [1]. In case of a point to point HVDC link, the fault is interrupted by the operation of the associated AC circuit breakers, leading to a zero power flow in the HVDC link. However, in case of a MTDC system with a large power infeed, in order to interrupt the fault, each terminal of the MTDC network should be disconnected when AC breakers are used. This results in complete de-energization of the DC grid. This will also affect the continuity of the power supply and is not economical. Hence, the DC breaker plays an essential role in MTDC systems as it provides complete selective fault isolation without affecting the power flow in the healthy DC lines. The DC CBs are classified in three groups, namely, mechanical, solid-state and hybrid DC CBs [2], [3]. Mechanical DC CB makes use of a series RLC resonate circuit to create an artificial current zero crossing, which is ultimately needed to interrupt a fault current. Mechanical CBs are further classified into active and passive ones. The active DC CB is faster as the fault interruption time is between 5 ms and 8 ms [2], whereas the current interruption time of the passive CBs is between 20 – 40 ms [2]. Among all the DC CBs, the solid-state breaker is fastest with a fault interruption time of less than 1 ms [3], [4], but has higher on-state losses. Hybrid HVDC circuit breaker consists of mechanical switch(es) and power electronics components. Thus, it is faster and has lower on-state losses. Over the years, different concepts of the hybrid breaker are presented and demonstrated, and nowadays, hybrid DC CBs interrupt the current within 5 ms [2]. In recent years, a novel DC breaker concept has been proposed, which is known as a VSC assisted resonant current (VARC) DC CB [5]–[7]. VARC DC CB makes use of voltage source converter (VSC) in combination with a resonating LC circuit to create high-frequency growing injected current oscillation in a vacuum interrupter (VI). The operating time of the VARC DC CB is 3 ms. The previous studies on VARC DC CB have only focused on the performance of the breaker in an MTDC network using a detailed model. Despite this, no studies have been so far realized related to the simplification of a detailed VARC model for system-level studies. Depending on the purpose of the study, the HVDC DC CB can be modelled by Electromagnetic transient simulation (EMT) based programs with different level of complexity. In order to identify the weak link within the DC CB, different critical components like the VIs, IGBTs, the surge arrester (SA) and the commutation elements (oscillation inductor and capacitor) should be studied for different types of faults. Moreover, the analysis can be performed by considering the detailed model of the HVDC breaker. However, due to the larger number of switching devices with a high switching frequency, the developed network is represented by a large admittance matrix. Hence, the detailed model is not recommended for system level studies with higher number of terminals as it requires large computational time and resources.

Therefore, this paper proposes an average VARC model, so the simulation time will be shorter than that of the detailed model without affecting the accuracy of the results. Furthermore, in order to demonstrate the effectiveness of the model, a comprehensive comparison between the detailed and the average model is performed. Based on this, the reader can make a deliberate decision to use an appropriate DC CB models for a particular study. Here, both models are implemented and simulated in PSCAD/EMTDC environment and compared in terms of their performance and simulation speed.

II. MODEL COMPARISON AND CALIBRATION

A. *Detailed model of VARC DC CB*

The detailed modelling of the VARC DC CB is discussed in [6],[7] and illustrated in fig. 1. The detailed model takes into account the three major branches, i.e. main branch, energy absorption branch and current injection branch. The main branch consists of a residual circuit breaker (RCB), a line inductor (L_{DC}) and a VI. The energy absorption branch is the SA and finally, the current injection branch consists of an oscillation inductor (L_P) and a capacitor (C_P) in series with a voltage source converter (VSC). In order to make use of this model for grid application studies, it needs to be connected in series to HVDC line or a cable.

This work has received funding from the European Commission under project 691714 – PROMOTioN (Progress on Meshed HVDC Offshore Transmission Networks) through Horizon 2020 program."

A. Shetgaonkar and M. Popov are with Delft University of Technology, Faculty of EEMCS, Mekelweg 4, 2628CD, Delft, The Netherlands (e-mail: A.D.Shetgaonkar@tudelft.nl; M.Popov@ieee.org)

S. Liu is with the State Key Laboratory of Electrical Insulation and Power Equipment, Department of Electrical Engineering, Xi'an Jiaotong University, 710049, Xi'an, China. (e-mail: S.liu-2@tudelft.nl).

2022 IEEE Power & Energy Society General Meeting (PESGM) | 978-1-6654-0823-3/22/$31.00 ©2022 IEEE | DOI: 10.1109/PESGM48719.2022.9916949

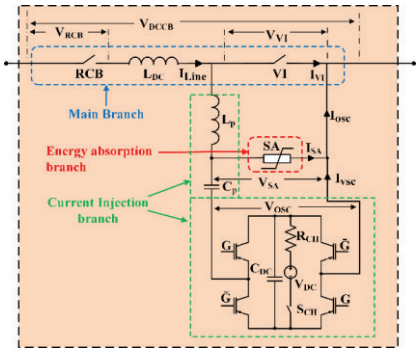

Fig. 1. Structure of VARC DC CB [7]

For a 320 kV grid application, the series connection of 4 modules of VARC DC CB with a rating of 80 kV is used. The detailed model of the VARC DC CB describes the effect of the parasitic components. In this model, the current interrupting devices (VI and RCB), the semiconductor switches ("G" and "$\bar{G}$") and the SAs are adopted from the PSCAD library.

The arc of the VI is not modelled, however, the non-linear characteristics of the components is taken into account by using piecewise linear method. Hence, the accurate voltage and the current stress can be observed not only at the component level but also at the system level. By applying detailed models, various aspects can be studied like the temperature and the energy dissipation in the SAs, and the switching losses. Furthermore, the modular topology of the VARC enables to determine the voltage distribution due to a delayed trip signal in each module [7]. Hence, the detailed model reflects the actual configuration of the model topology, i.e. whether it is a modular or a series-connected VI topology. The main drawback of the detailed VARC DC CB model is that simulating electrical circuits with non-linear elements takes considerable amount of time.

III. An Average Model Of VARC DC CB

The principle of operation and the average model is illustrated in Fig. 2 (a-d). Similar to the detailed model, the average model has three major branches. During the fault neutralisation time (Fig. 2 (a)), the VIs of the modules conduct; hence it can be represented by a single switch from the PSCAD/EMTP database. The voltage rating of this switch will be equivalent to the system voltage. At the beginning of the fault current suppression time, the line current is commuted to the current injection branch. As a result, all the oscillation capacitors of the modules are connected in series, as shown in Fig. 2 b. Hence, the entire configuration is represented by a single capacitor. Furthermore, the value of this capacitance is equal to the equivalent series capacitance of the module's oscillation capacitor, which is computed by (1).

$$C_{P_{eq}} = \frac{C_P}{N_m} \tag{1}$$

where C_P denotes an oscillation capacitor of a module and N_m is the number of modules. Due to the presence of an equivalent oscillation capacitor, the interaction of this capacitor with the system can be analysed after the fault interruption.

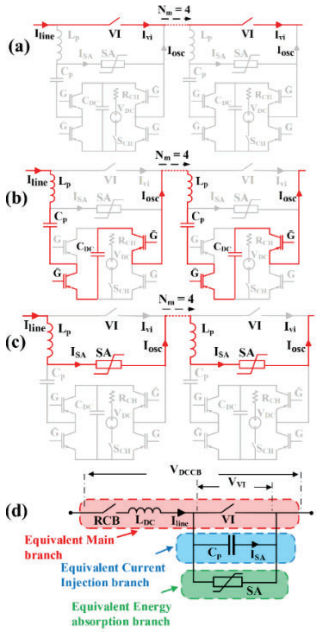

Fig. 2. Flow of line current in a VARC DC CB. (a) During fault neutralisation time, (b) During rise of TIV, (c) During fault current suppression time and (d) Average model of VARC DC CB

However, the oscillation inductance is omitted in the average model. As the clamping voltage of the SA in the detailed model is achieved, the line current is commuted to the energy absorption branch as presented in fig. 2 (c). Hence, during this period all the SAs of the modules are connected in series. As a result, a single SA represents the series connected SAs with a system voltage rating. Table I, provides the data of the detailed and the average model of a 320 kV system. The VI and the RCB in this model are modelled as ideal switches. This switch has two states, ON state with a low resistance value, and OFF state with a high resistance value. Furthermore, the switch is set to operate near current zero. Hence, this switch is accurate and reduces the computation time as the complexity of equation is reduced.

TABLE I
Parameter of Detailed and Average VARC Model For 320 kV System

Parameter	Symbol	Detailed model	Average model
Oscillation inductor	L_P	95 μH	0 μH
Oscillation Capacitor	C_P	2.72 μF	0.68 μF
Rated / clamping voltage of SA	-	80/120 kV	320/480 kV
Initial Voltage across C_P	V_{iniCP}	10 kV	0 kV
Number of modules	Nm	4	1

Line inductor (L_{DC}) is considered as the linear electrical component. However, the SA is modelled as a non-linear element in PSCAD environment. In PSCAD, the SA makes use of a Piecewise Linear Method, which reduces the order of the conductance matrix and the inversion per run is with a reasonable accuracy. Moreover, the details of the parasitic and the grading components are ignored in the average model. Despite the simplification of the current injection branch, an average VARC model provides high accuracy in terms of energy absorption and conduction losses in SA and VI respectively compared to a detailed model.

978-1-6654-0823-3/22/$31.00 ©2022 IEEE

IV. 4-TERMINAL MTDC SYSTEM

Fig. 3 illustrates a 4-terminal test MTDC system, which is used for the fault current interruption analysis. The converters are half-bridge modular multilevel converters (MMC). The entire MTDC system is divided into two zones, onshore and offshore. The onshore part consists of MMC 1 and MMC 2, which are then connected to the 400 kV AC grid via a transformer. The offshore grid consists of MMC 3 and 4, which are connected to the wind farms. The onshore AC grids are independent voltage sources. The MTDC system is configured as a symmetrical monopolar with ±320 kV dc voltage. The parameters of the MTDC system are indicated in Table II.

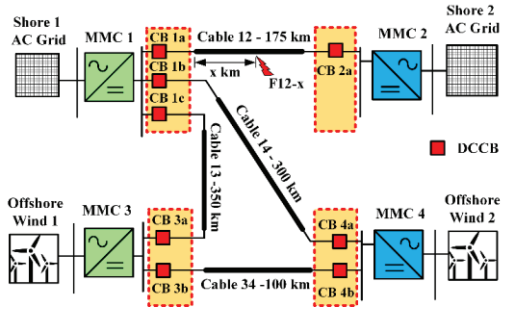

Fig. 3. 4 - Terminal MTDC system

There are four cables connecting the Onshore and Offshore zone. Cable 12 with a length of 175 km connects MMC 1 and MMC 2. MMC 3 is connected by a 350 km long cable to MMC 1, whereas another offshore zone MMC is connected to MMC 1 through a 300 km long cable. Both offshore MMCs are connected through a 100 km long cable. The DC reactor, with the value of 10 mH, is installed between MMC and the bus. At each bus, as indicated by a red dotted rectangle, a DC CB is installed. The value of the line inductor is 100 mH [8]. This system uses 320 kV XLPE insulated cable with a characteristic impedance of 33.73 Ω and a wave propagation velocity is $1.83 \times 10^8\, m/s$. The frequency-dependent phase model is used to represent the cable in a PSCAD environment. The MMC used in this system is an average value MMC model. The outer control loop of the MMC 1 and 3 controls the voltage, whilst MMC 2 and 4 controls the power. The MMC utilizes two protection strategies; firstly, MMC blocks, when the maximum arm current exceeds the 0.8 times the maximum current handling limit of the IGBT and secondly MMC blocks when the MMC voltage falls below 0.8.p.u.

TABLE II
DATA OF 4- TERMINAL MTDC SYSTEM

Parameter	Converters			
	MMC 1	MMC 2	MMC 3	MMC 4
Active power	500 MW	500 MW	500 MW	500 MW
Control mode	PVdc	PVdc	PQ	PQ
Reactive power	100 MVAR	100 MVAR	100 MVAR	100 MVAR
DC link Voltage	±320 kV			
Rated power	1256 MW			
Number of Submodules per arm	400			
Arm capacitance C_{arm}	22 µF			
Arm indcutance L_{arm}	42 mH			
Arm resistance R_{arm}	0.544 Ω			
AC converter voltage	400kV			
Transformer leakage reactance	0.18 p.u			
AC grids and windfarms				
AC grids voltage	400 kV			

V. MODEL PERFORMANCE AND VALIDATION

A comparison of the two different models of the VARC DC CB is made based on different technical performance. Both DCCB models have a current interrupting functionality as they are able to interrupt a nominal fault current. The average model shows similar technical performance with the detailed model. However, for some scenarios there is a small margin of error, for example in case of the nature of the injected oscillating current. In the detailed VARC model, the amplitude of the injected oscillation current changes after each reversal, whereas due to the lumped capacitor (C_P) in the average model, this growing oscillation is absent. Besides, the average model loses some component level information like VSC's voltage and current stress, voltage sharing and redundancy, and the scaled topology information. Additionally, the average model can provide necessary information on the estimation of the SA energy absorption, VI power loss estimation and fault interruption capability. In order to verify this, two transient studies are performed.

A. Terminal short circuit at MMC 1

In the first study, a pole-to-pole fault is applied at the terminal of MMC 1 in cable 12. Initially, the system is in the steady-state condition with a steady state current of 0.87 kA. At the instant of 1 s, a fault is applied, and as a result, the fault current rises with a rate of 2.9 kA/ms. Fig. 4 shows the current and the voltage response of the detailed and the average VARC DC CB model during this terminal short circuit for the positive pole. Both models show an identical overlap of the voltage across the DC CB during a fault current interruption. Similarly, both models provide information about post fault interrupting oscillation. The cause of this oscillation is due to the interaction of the system inductance and oscillation capacitor (C_P) of both models. The frequency of this oscillation is $f = \frac{1}{2\pi\sqrt{LC}} = \frac{1}{2\pi\sqrt{110mH \times \frac{2.72\mu F}{4}}} = 580Hz$. Furthermore, due to higher damping components, the detailed model has a lower peak of this oscillation. In both models, the oscillation capacitor (C_P) determines the rate of rise of TIV. Also, both models have information about the TIV during the fault current suppression time, and the peak value is 1.5 times the rating of a SA.

In the detailed model, without considering the losses in the DC CB, the peak value of the injected current is expressed as follows:

$$I_{OSC_{pk}} = \frac{(N+2) \times V_{DC}}{\sqrt{\frac{L_P}{C_P}}} \qquad (2)$$

where N is the number of reversals within the VSC. In order to reach the fault current amplitude of 8.74 kA, four reversals take place in the VSC. Hence, after four reversals, the expected peak amplitude of the injected current will be 10.15 kA.

978-1-6654-0823-3/22/$31.00 ©2022 IEEE

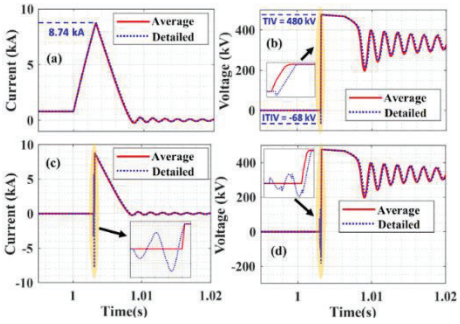

Fig. 4. Comparison of VARC models during a Pole to pole fault on cable 12 near converter station 1.(a) CB 12 Line Current (kA) (b) CB 12 Voltage (kV) (c) CB 12 injected current (kA) (d) CB 12 SA Voltage (kV)

However, due to the lower fault current, the current in the VI is interrupted at the non-peak value of the injected current. As a result, ITIV with the amplitude of -68 kV is developed across the VI, which can be theoretically computed by

$$V_{ITIV} = N_m \times (N+1) \times V_{DC} \cos\theta \quad (3)$$

$$\theta = \sin^{-1}\left(\frac{I_f}{I_{OSC_{pk}}}\right) \quad (4)$$

Here, N_m is the number of VARC modules, and the theoretical value of ITIV is about 30% higher than that of the simulated value due to the resistive losses. The average model of VARC does not provide information about the ITIV as observed in fig. 4. Similarly, the information about the nature of the injected current is absent. However, the average model accurately follows the envelope of the detailed model with a small error for the voltage and the current, as indicated in Table III. There is an energy difference of 0.2 MJ between the average and the detailed model. This energy difference results from the extra time taken by the injected current to reach the peak current value of the fault current, as shown in Fig. 5 (a). The following steps can theoretically calculate this extra time: The injected current is given by:

$$I_{OSC} = I_{OSC_{pk}} \times \sin(\theta) \quad (5)$$

TABLE III
PERCENTAGE OF ERROR OF AVERAGE MODEL FROM DETAILED MODEL DURING TERMINAL SHORT CIRCUIT AT MMC1

Signals	% of Error
Line Current	1.18
Voltage across DC CB	0.12
Injected Current	1.17
Voltage across SAs	0.04

At the end of fault neutralisation time, $I_{OSC} = I_f$. Thus for given $\theta = 60°$and extra time, $t = \frac{0.1ms \times 60°}{360°} = 1.5 \times 10^{-5}\ s$.

The energy difference can be calculated by the current flowing through the SA and the voltage across the SA during the energy absorption period. By taking into account that the rate of rise of the fault current is 2.9 kA/ms and assuming a constant value of SA voltage and current during fault current suppression time, the estimated energy absorbed by the average model is $E_{SA_{avg}} = 4 \times 8.7kA \times 120kV \times 5ms = 20.8MJ$. Similarly, in the detailed model, the energy absorbed by the SA is $E_{SA_{det}} = 4 \times (8.7kA + 2.9kA/ms \times 1.5 \times 10^{-5}) \times 120kV \times (5ms + 1.5 \times 10^{-5}) = 21.0MJ$. Hence, the net difference in both models for the SA energy is 0.2 MJ.

Fig. 6 (a) illustrates MMC 1 positive pole bus voltage during a terminal short circuit for both models. The fault occurs at 1s, and thereafter, the voltage of MMC1 bus drops to 270 kV. It further reduces, as the MMC 1 current rises as seen from Fig. 6 (a) and (c). The reduction rate of the bus voltage is defined by the value of the line inductance. Next, with the operation of the DC CB at 1.003 s, a spike is observed only in the detailed model, which represents the ITIV. Due to the TIV, the bus voltage starts to recover. However, after the current zero takes place in the VI, the bus voltage is affected by a superimposed voltage oscillation of 580 Hz, which results from the interaction of C_P and system inductance, as explained in the previous paragraphs. Moreover, this oscillation is eliminated with the operation of the residual circuit breaker (RCB). During the entire fault scenario, the MMC remains unblocked, as the protection criteria are not violated. Furthermore, the MMC 1 positive pole current, reaches 4.4 kA at 1.003 s, after which it drops with a rate determined by the clamping voltage. However, the MMC remains in operation after current interruption as the only faulty line is isolated. The positive pole cable voltage seen from both MMC's i.e 1 and 2, yields similar results for both models. Moreover, the cable voltage seen from MMC 2 oscillates (fig. 6 (d) due to the travelling wave reflections occurring during the transient event.

B. *Steady-state current interruption*

In this study case, a switching action is carried out in cable 12. The MTDC system again operates in a steady-state condition with a line current of 0.87 kA in cable 12. Then, at 1 s, a switching action is carried out in cable 12 by sending a trip signal to CB 1a and CB 2a. For the lower current interruption, only the main branch and the current injection branch interact with the system. This occurs as the current level is lower; the voltage across the oscillation capacitor (C_P) is lower than the clamping voltage of SA (i.e 480 kV); therefore, the energy absorption branch does not contribute in current interruption. Hence, the line current for both models oscillates with the frequency of 580 Hz after the fault is interrupted as previously explained. The VARC DC CB is primarily designed to interrupt the rated fault current. Thus, with the first reversal of the VSC voltage, the peak value of the injected current given by (2) is 3.3 kA (Fig. 7 (c)). Besides, due to the higher value of the $I_{OSC_{pk}}$, corresponding ITIV is higher. The value of the ITIV can be estimated by (3) and (4) with N = 1, which results in a voltage of -155 kV. The resistive losses cause about 3% lower value of ITIV in the simulated result than that in the analytical result.

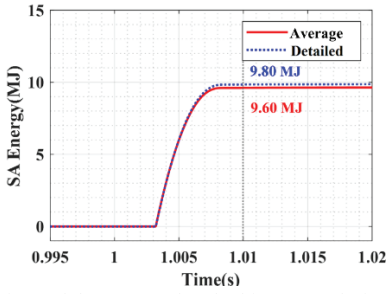

Fig. 5. Comparison of the energy absorbed in CB 1a during a terminal short circuit for both the average and the detailed VARC model

978-1-6654-0823-3/22/$31.00 ©2022 IEEE

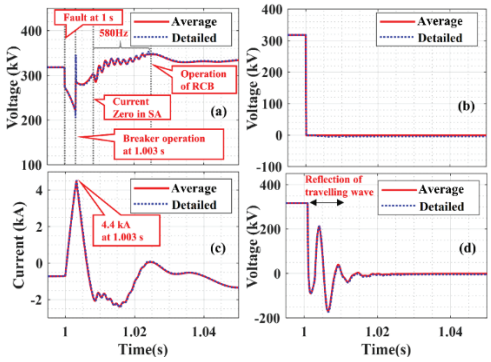

Fig. 6. Average and detailed model comparison during a pole-to-pole fault on cable 12 near converter station 1 in Positive pole (a) bus voltage (kV) (b) Cable voltage observed from MMC 1 (kV) (c) MMC 1 current (kA) and (d) cable voltage observed from MMC 2 (kV)

However, due to the equivalent representation of the current injection branch in the average model, the details about $I_{OSC_{pk}}$ and ITIV are missing. Similarly, the voltage stress information about the SA is omitted. Throughout the entire transient study, the anticipated results by the average model remains in great harmony concerning the reference solution provided by the detailed model. For the low current interruption, the current and the voltage signals in the average model show an identical curve profile with deviations as shown in Table IV.

VI. COMPUTATIONAL TIME

The 4-terminal HVDC system is simulated for a duration of 1.2 s using the detailed and the average model at two different time steps. With the average value MMC model in the 4-terminal HVDC system, the simulation can be run with higher time steps and yet maintaining acceptable accuracy. This HVDC system can be simulated with a time step of 2 - 10 µs, without losing its dynamic response. For the detailed VARC model, accurate results can be achieved with a time step lower than 2 µs. Hence, the detailed model creates a bottleneck in the system. As a result, the overall time step is reduced for the accurate transient and steady-state response.

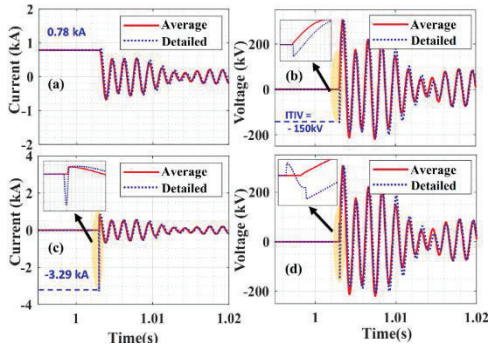

Fig. 7. Comparison of VARC models during steady-state current interruption in cable 12 (a) CB 12 line Current (kA) (b) CB 12voltage (kV) (c) CB 12 injected current (kA) (d) CB 12 SA voltage cable voltage observed from MMC 2 (kV)

Due to the reduction in the admittance matrix, the average VARC model can be simulated with a higher time steps without violating the transient response. The preferred time step for the average model is at most 10µs for the studied HVDC system. The comparison of the simulation time for the two models is summarized in Table V. As it can be seen from Table V, the average model performs with much lower simulation time compared to the detailed model.

TABLE IV
PERCENTAGE OF ERROR OF AVERAGE MODEL FROM DETAILED MODEL DURING STEADY-STATE CURRENT INTERRUPTION

Signals	% of deviation
Line Current	3.55
Voltage across DC CB	0.94
Injected Current	3.51
Voltage across SAs	0.68

TABLE V
COMPARISON OF COMPUTATION TIME OF DIFFERENT MODELS FOR TIME INTERVAL FROM T = 0 S TO T = 1.2 S

Model	Time step	Simulation time
Detailed model	2 µs	22 min
Average model	10 µs	3 min

VII. CONCLUSION

This paper presents a comparative study of two different model representation of VARC DC CB technology, namely, detailed and average model in PSCAD environment. The performance of the proposed average and the detailed model are examined analytically and by simulation, for the low and high current interruption. The presented results show that the average model provides a good level of accuracy during the steady-state and the transient condition with respect to the detailed model. The significance of the average model is that, it reduces the simulation time by 86% compared to the detailed model, thereby enabling the average model for system-level simulation studies. This makes the average computationally efficient and attractive. Deviation percentage during a terminal short circuit is lower than that during a low current interruption. Furthermore, the module's components information are not provided by the average model. Similarly, the details of the ITIV and the scaling information are also absent. The model can also be easily developed in real-time simulator and it can be successfully used for protection studies as the current amplitude, the duration and the rate of rise can be accurately determined.

VIII. REFERENCES

[1] S. S. Mirhosseini, S. Liu, J. C. Muro, Z. Liu, S. Jamali, and M. Popov, 'Modeling a voltage source converter assisted resonant current DC breaker for real time studies', *Int. J. Electr. Power Energy Syst.*, vol. 117, p. 105678, 2020.

[2] C. M. Franck, 'HVDC Circuit Breakers: A Review Identifying Future Research Needs', *IEEE Trans. Power Deliv.*, vol. 26, no. 2, pp. 998–1007, 2011.

[3] E. Kontos, R. T. Pinto, S. Rodrigues, and P. Bauer, 'Impact of HVDC Transmission System Topology on Multiterminal DC Network Faults', *IEEE Trans. Power Deliv.*, vol. 30, no. 2, pp. 844–852, Apr. 2015.

[4] C. Meyer, S. Schroder, and R. W. De Doncker, 'Solid-state circuit breakers and current limiters for medium-voltage systems having distributed power systems', *IEEE Trans. Power Electron.*, vol. 19, no. 5, pp. 1333–1340, 2004.

[5] L. Ängquist, S. Nee, T. Modeer, A. Baudoin, S. Norrga, and N. A. Belda, 'Design and test of VSC assisted resonant current (VARC) DC circuit breaker', in *15th IET International Conference on AC and DC Power Transmission (ACDC 2019)*, 2019, pp. 1–6.

[6] L. Ängquist, A. Baudoin, T. Modeer, S. Nee, and S. Norrga, 'VARC – A Cost-Effective Ultrafast DC Circuit Breaker Concept', in *2018 IEEE Power & Energy Society General Meeting (PESGM)*, 2018, pp. 1–5.

[7] S. Liu., M. Popov, S. Mirhosseini, S. Nee, T. Modeer , L. Ängquist, N A. Belda, K. Koreman and M Van Der. Meijden, 'Modelling, Experimental Validation and Application of VARC HVDC Circuit Breakers', *IEEE Trans. Power Deliv.*, p. 1, 2019.

[8] S. Liu, A. Shetgaonkar, and M. Popov, 'Coordinative performance of HVDC circuit breakers in MTDC grids', presented at *IEEE Power Engineering Society General Meeting, 2020.* .

978-1-6654-0823-3/22/$31.00 ©2022 IEEE